Polar confinement of a macromolecular machine by an SRP-type GTPase

Anita Dornes[1,#], Lisa Marie Schmidt[2,#], Christopher-Nils Mais[1], John C. Hook[2], Jan Pané-Farré[1], Dieter Kressler[3], Kai Thormann[2*], and Gert Bange[1,4*]

[1]Philipps-University Marburg, Center for synthetic Microbiology (SYNMIKRO) and Department of Chemistry, Hans-Meerwein-Strasse 6, C07, 35043 Marburg, Germany
[2]Justus-Liebig-Universität, Department of Microbiology and Molecular Biology, Heinrich-Buff-Ring 26, 35392 Giessen, Germany
[3]University of Fribourg, Department of Biology, Chemin du Musée 10, 1700 Fribourg, Switzerland
[4]Max-Planck-Institute for terrestrial Microbiology, Molecular Physiology of Microbes, Karl-von-Frisch Strasse 14, 35043 Marburg, Germany

[#]These authors contributed equally to this work.
*Correspondence:
gert.bange@synmikro.uni-marburg.de
kai.thormann@mikro.bio.uni-giessen.de

Significance statement.
Flagella serve as bacterial locomotion organelles, with their number and location, known as the flagellation pattern, being species-specific and among the earliest taxonomic criteria in microbiology. Bacteria replicate their flagellation pattern with each cell division. Flagella localization and abundance depends on the SRP-type GTPase FlhF, together with its regulator FlhG. Our study clarifies the mechanism through which FlhF coordinates the polar positioning of the flagellum, working in tandem with the polar landmark protein HubP and aiding in the assembly of flagellar MS-ring/C-ring components at the cellular pole.

Abstract
The SRP-type GTPase FlhF, along with its regulator FlhG, orchestrates the localization and quantity of flagella in bacteria. Our study reveals that FlhF anchors developing flagellar structures to the polar landmark protein HubP/FimV, thereby restricting their formation to the cell pole. Specifically, the GTPase domain of FlhF interacts with HubP, while an as-yet-uncharacterized structured domain at the N-terminus of FlhF binds to FliG. This FlhF-bound FliG subsequently engages with the MS-ring protein FliF, but not with the C-ring proteins FliM/FliN. Consequently, FlhF's interaction with HubP/FliG recruits a functional FliF/FliG complex to the pole, while FlhG's modulation of FlhF controls FliG's interaction with FliM/FliN, thereby regulating the progression of flagellar assembly at the pole.

INTRODUCTION

The flagellum is a macromolecular machine, which enables the movement of bacteria along chemical gradients (1). The core flagellar architecture is conserved, and it is composed of the MS-ring, cytoplasmic C-ring, the rod, and extracellular hook and filament (**Fig. 1a**). The membrane-embedded MS-ring is formed by multiple copies of a single transmembrane protein FliF (2-5). At the cytoplasmic side of the MS-ring resides the flagellar C-ring, an oligomeric structure of the proteins FliG, FliM and FliN (6, 7), and required for power transmission, in both counter-clockwise and clockwise rotational modes of the flagellum.

The number and arrangement of flagella give rise to unique "flagellation patterns," which vary between bacterial species but remain characteristic to each (8-10). However, the molecular mechanisms controlling the spatial-numerical distribution of flagella are still far from being understood. The FlhF protein, in conjunction with the MinD-type ATPase FlhG, also referred to as YlxH, FleN, MotR, or MinD2, plays a crucial role in determining the positioning and assembly of flagella in numerous polar and peritrichous flagellated bacteria (reviewed in: (8, 9)). FlhF is essential for directing the initial flagellar protein, FliF, to the cell pole, although the exact mechanism remains incompletely understood (11, 12).

FlhF belongs to the family of signal recognition particle (SRP)-GTPases, and shares its NG-domain with the other two members of the family (i.e., Ffh and FtsY) (13, 14). The GTPase activity of FlhF is stimulated by FlhG, through a conserved "DQAxxLR" motif present at its N-terminus (15, 16). In contrast to the other two SRP-GTPases, FlhF possesses an N-terminal B-domain believed to be structurally disordered and implicated in the targeting of FliF (**Fig. 1b**; (11, 12)). In addition, we recently identified a FlhF-interacting protein, named FIP, which is involved in targeting FlhF to the cell pole in *Vibrio parahaemolyticus*, *Pseudomonas putida* or *Shewanella putrefaciens* (17). However, the molecular mechanism by which FlhF enables assembly of the flagellum at one cell pole in monotrichous bacteria is still elusive.

Thus, we set out to shed light on the molecular mechanism enabling FlhF to position the flagellum in polar flagellates. To this end, we used *S. putrefaciens* CN32 as our model system, in which we have previously studied in detail the flagellar regulation, mechanism and function of FlhG (18-20). *S. putrefaciens* harbors two distinct flagellar systems (21, 22) (**Fig. 1c**). The primary main monopolar system depends on FlhF and FlhG, while the secondary lateral system is not affected by these two proteins. Our data show that FlhF initiates polar flagellar assembly by facilitating assembly of the flagellar MS-ring assembly by directing a key protein of the cytoplasmic C-ring, FliG, to the designated position.

RESULTS

The B-domain of FlhF interacts with FliG in the polar flagellar system, excluding the lateral system. FlhF has been suggested to guide the MS-ring protein, FliF, toward the cell pole (11, 12), albeit a molecular mechanism remains elusive. These studies suggested to us that FlhF might execute its function in the context of the MS- and/or C-ring proteins FliF, FliG, FliM and FliN (**Fig. 1a**).

Thus, we started by conducting a yeast-two-hybrid (Y2H) screen using the *S. putrefaciens* proteins with FlhF as the bait protein and FliF, FliN, FliM, or FliG as the prey proteins. Since FliF is a membrane protein, we employed its cytoplasmic domain

1 (FliF-C). The results showed that while FlhF did not interact with FliF-C, FliM, or FliN, it
2 exhibited a strong interaction with FliG (**Fig. 1d**). To validate this discovery, we also
3 assessed the interaction between FlhF and FliG from the lateral flagellar system (FliG-
4 Lat).
5 Contrary to the robust interaction between FlhF and FliG from the polar system, no
6 Y2H interaction could be observed between FlhF and FliG-Lat (**Fig. 1d**). Consequently,
7 we conclude that FlhF specifically interacts with FliG from the polar flagellar system in
8 *S. putrefaciens*, while not engaging with the FliG protein lateral flagellar system.
9 Earlier experiments have indicated that the B-domain of FlhF plays a critical role in the
10 polar targeting of FlhF (11, 12). Consequently, we conducted a Y2H analysis to
11 determine whether the B-domain could interact with FliF-C, FliM, FliN, or FliG. Our
12 results clearly demonstrate that the B-domain is both necessary and sufficient for the
13 interaction between FlhF and the C-ring protein, FliG (**Fig. 1e**). Notably, similar to the
14 full-length FlhF protein, the B-domain exhibits selectivity, distinguishing between FliG
15 proteins of the polar and lateral flagellar systems (**Fig. 1e**).
16
17 **A structured domain at the N-terminus of FlhF mediates the FliG interaction.** To
18 consolidate the interaction of the FlhF B-domain with FliG at the biochemical level, we
19 recombinantly produced a StrepII-tagged B-domain together with FliG in *Escherichia*
20 *coli* BL21(DE3) and performed a pulldown from the cleared cell lysates. The
21 experiment shows a stoichiometric interaction between FlhF-B and FliG (**Fig. 2a**, *first*
22 *lane*). In the next step, we performed the same experiment probing the ability of
23 different B-domain truncations to interact with FliG. Only when the first 60 amino
24 acids of the B-domain were fully present, an interaction with FliG could be observed
25 (**Fig. 2a**, *second lane*). These data show that the N-terminal 60 amino acids are
26 necessary and sufficient for the interaction of FlhF and FliG (**Fig. 2a**).
27 Structural analysis by X-ray crystallography of a FlhF construct encompassing the first
28 60 amino acid residues showed that residues 1 to 46 of the B-domain form a domain
29 consisting of three anti-parallelly arranged β-strands and one α-helix (**Fig. 2b**,
30 **Supplementary Table 1**). These data show that the N-terminus of the B-domain, which
31 provides the FliG-interaction site of FlhF is structured. Due to its adept interaction with
32 FliG, we propose labeling this domain as the FliG Interaction Domain (FID).
33 We also wanted to gain a better understanding of which part of FliG would be required
34 for the interaction with FlhF. Structural analysis showed that FliG consists of three
35 domains, the N-terminal (FliG-N), a middle (FliG-M), and a C-terminal domain (FliG-C).
36 As each of the three domains alone is not stable at the biochemical level, we decided
37 to employ two FliG variants containing either the N- and M-domains (FliG-NM) or the
38 M- and C-domains (FliG-MC) (**Fig. 2c**, *upper panel*). Again, we performed pulldown
39 assays with a StrepII-tagged FlhF as bait and FliG, FliG-NM or FliG-MC as prey. FlhF
40 shows a stoichiometric interaction with FliG and FliG-MC, however, its interaction with
41 FliG-NM appeared sub-stoichiometric (**Fig. 2c**, *lower panel*). These data strongly
42 suggest that the interaction site of FlhF resides within the M- and C-domains of FliG.
43 Analytical size exclusion chromatography confirmed the interaction between FlhF-B
44 and FliG-MC (**Fig. 2d**).
45 As the next step, our aim was to gain a deeper understanding of the consequences
46 stemming from the FlhF/FliG interaction. Specifically, we sought insights into two
47 aspects: firstly, its impact on the interaction between FliG and the MS-ring protein

FliF, and secondly, its influence on FliG's ability to engage with its C-ring counterparts, FliM and FliN. When bound to FlhF, FliG was able to interact with the cytoplasmic domain of the flagellar MS-ring forming protein FliF (**Fig. 2e**). Nevertheless, upon binding to FlhF, FliG exhibited an inability to interact with FliM/N (**Fig. 2f**). These observations underscore that FlhF acts as an impediment, hindering the interaction between FliG and its C-ring partners FliM/FliN, while allowing engagement of FliG to FliF.

FlhF-GTPase interacts with the cytoplasmic region of HubP. The FlhF-FID interaction with FliG raises the question in which functional context FlhF operates at the cell pole. Previous studies have suggested that FlhF can interact with the polar landmark protein HubP, a hub for various protein interactions (16, 23, 24). However, a deeper molecular picture is elusive. HubP is a transmembrane protein with an N-terminal LysM-type domain, followed by a transmembrane segment and an extended cytoplasmic region of approximately 70 kDa (HubP-C) (**Fig. 3a**). An Alpha2-fold prediction of HubP including HubP-C is widely unsatisfactory (**Supplementary Fig. 1**), and predicts the presence of a TPR-repeat, which has been structurally determined for the *Pseudomonas aeruginosa* HubP/FimV (25).

To investigate whether FlhF would interact with the cytoplasmic region of HubP (HubP-C), we designed several HubP variants. However, we could only produce variants starting from amino acid 860 to the C-terminus of the protein. For the pulldowns, FlhF as prey and different StrepII-tagged version of these HubP-C variants were used as baits (**Fig. 3a**). This experiment shows that FlhF interacts with HubP-C, in a region involving residues 860 – 1033, not including the C-terminal TPR domain (**Figs. 3b**). We also probed which of the FlhF domains would be necessary for the FlhF-HubP interaction. We show that the NG domain of FlhF is required for the interaction with HubP-C, while the B-domain is not (**Fig. 3c**).

Next, we probed whether the interaction of NG-FlhF and HubP-C would depend on the presence of nucleotides. Therefore, we performed *in vitro* pulldown assays probing whether the addition of GDP or GTP would affect the interaction of NG-FlhF with an StrepII-tagged HubP-C variant immobilized on beads (**Fig. 3d**). This experiment shows that neither GDP nor GTP affect the NG-FlhF/HubP-C interaction. This notion is supported by GTP hydrolysis assays showing that HubP-C does not affect the GTPase activity of NG-FlhF, in stark contrast to the FlhF-GTPase stimulating protein FlhG (**Fig. 3e**). Taken together, we show that the NG domain of FlhF interacts with the C-terminal cytoplasmic region of HubP in an apparently nucleotide-independent manner without affecting the GTPase activity of FlhF.

FlhF can bring FliG into the proximity of HubP. We have shown that FlhF can interact with the C-ring protein FliG and the polar landmark protein HubP through its FID- and NG-domains, respectively. In a next step, we wanted to study whether both interactions would be possible at the same time. Therefore, StrepII-tagged HubP-CR was used as bait and FlhF and FliG as prey. As shown above, FlhF interacted with HubP-CR, and when FliG was added a stoichiometric complex of the three proteins was observed (**Fig. 3f**). This result shows that FlhF is able to bridge HubP and FliG *in vitro*. These data allow a hypothesis in which the NG-domain of FlhF mediates interaction

4

1 with the polar landmark HubP, while the first 44 N-terminal residues of FlhF B-domain
2 interact with FliG to initiate flagellar formation.
3 If correct, we anticipate that a FlhF variant lacking its N-terminal FliG-binding region
4 would still localize to the cell pole, while simultaneously loosing capability to recruit
5 FliG. We therefore determined the localization of a ΔN44-FlhF mutant *in vivo* and its
6 effect on flagellar positioning. For this purpose, we utilized a *S. putrefaciens* strain
7 with a chromosomal fusion of mVenus to *flhF* (*flhF*-mVenus) (16), wherein we
8 specifically deleted the N-terminal 44 residues of the *flhF* gene (*flhF*ΔN44-mVenus).
9 Furthermore, we labeled the hook structures of the strain by introducing a T183C
10 substitution in the flagellar hook protein FlgE1, allowing for the coupling of maleimide-
11 ligated fluorescent dye (17). Importantly, the N-terminally truncated FlhF-mVenus
12 was consistently produced at levels comparable to the wild-type (**Supplementary Fig.**
13 **2**).
14 Fluorescence microscopy revealed fewer cells producing ΔN44-FlhF-mVenus
15 displayed fluorescent foci (about 70% compared to about 90% of full-length FlhF-
16 mVenus; **Fig. 4a**). However, these foci were always located at the cell pole (**Figs. 4a,b**).
17 In contrast, in the majority of ΔN44-FlhF mutant cells single flagellar hooks appeared
18 in subpolar/lateral positions (about 40%, 10% polar; **Figs. 4c,d**), while they exclusively
19 appeared at the cell pole in about 75% of wild-type cells (**Figs. 4c,d**). Accordingly, a
20 ΔN44-FlhF mutant phenocopies a *ΔflhF* mutant with respect to spreading through soft
21 agar (**Supplementary Fig. 3**). The analysis confirmed the hypothesis that ΔN44-
22 mutants of FlhF retain their ability to localize FlhF to the cell pole, but uncouple FlhF
23 localization from that of the flagella machinery.
24 *Vice versa*, we also tested whether localization of FlhF is affected in the presence or
25 absence of FliG as interaction partner. To this end, we used fluorescence microscopy
26 on a *S. putrefaciens* strain producing mVenus-labeled FlhF (FlhF-mVenus) bearing an
27 N-terminal (Δ2-85 aa; FliG ΔN) or a C-terminal (Δ209-348 aa; FliG ΔC) deletion in FliG.
28 Both deletions in FliG resulted in a pronounced accumulation of FlhF-mVenus at one
29 (about 60 %) or both cell poles (**Figs. 4a,b**) compared to wild type-background, which
30 exclusively exhibit monopolar localization in about 92 % of the cells (**Fig. 4b**). The
31 amount of polar fluorescence is also reflected in the amount of FlhF-mVenus protein
32 produced in the cells (**Supplementary Figs. 4a,b**). These findings suggest that coupling
33 to FliG and/or initiation of flagellar assembly is required to regulate FlhF accumulation
34 at the cell pole.
35

36 **The Shewanella HubP-FlhF-FliG recruitment cascade can be rebuilt in *E. coli*.** So far,
37 our findings suggested that, in *S. putrefaciens*, flagellar synthesis is initiated with FliF
38 being localized to the cell pole by the polar landmark protein HubP, to where it then
39 recruits FliG. If correct, this recruitment cascade may also be rebuilt in *Escherichia coli*,
40 which lacks orthologs to HubP and FlhF. To test this, fluorescently tagged or wild type
41 versions of HubP, FlhF and FliG were ectopically produced either alone or in
42 combinations from suitable expression plasmids in *E. coli* DH5α. As previously
43 observed (16), HubP-sfGFP localized to the polar regions of the cells and particularly
44 accumulated in the cell division plane (**Fig. 5a**). FlhF-mVenus produced alone formed
45 small monopolar and sometimes subpolar clusters in the cells. However, when
46 expressed in concert with HubP, FlhF also appeared bipolarly and frequently occurred
47 in the cell division planes, which was never observed in the absence of HubP (**Fig.**

5a,b). mVenus-FliG expressed alone could not be detected in the cells. In the presence of FlhF, small clusters of mVenus occurred in mono-, bi- and subpolar positions. In the additional presence of HubP, mVenus-FliG formed clusters at the cell poles and division planes (**Fig. 5a,c**), strongly indicating that HubP is able to recruit both proteins also in *E. coli*. The absence of a mVenus-FliG fluorescent signal in the absence of FlhF suggested that the latter may stabilize FliG. Correspondingly, western blotting showed that mVenus-FliG is only stable in the presence of FlhF, but not alone or in the presence of HubP (**Supplementary Fig. 5**), at least in the heterologous host *E. coli*. This may suggest that FliG requires stabilization by FlhF during flagellar assembly.

Discussion

In this study, we aimed at gaining a deeper mechanistic understanding of how the SRP-GTPase FlhF enables the polar localization of a flagellum in the polar flagellated bacteria, such as *S. putrefaciens* or Vibrio species. Previous studies have indicated that FlhF might act in the context of the flagellar C-ring, and proposed that FlhF establishes the site of flagellum assembly at the old cell pole membrane by recruiting the earliest flagellar structural component FliF (11, 12, 26). It might therefore be involved in assembly of the flagellar C-ring (27). However, the precise mechanism by which FlhF acts in the context of C-ring assembly, and whether FlhF would directly or indirectly interact with FliF was not known. Furthermore, it raised the question of whether any interaction between FlhF and the flagellar C-ring alone is adequate to fully explain how FlhF establishes polar localization of the flagellum.

In this study, we demonstrate that the multidomain protein FlhF, comprising an N-terminal B-domain followed by an SRP-type GTPase domain (aka: NG domain), both being connected by a linker region (**Fig. 2b**), can serve as a tether between the polar landmark protein HubP/FimV and the developing flagellar structure. While the NG domain of FlhF interacts with the C-terminal domain of the landmark protein HubP, a structured domain at the very N-terminus of its B-domain interacts with the flagellar C-ring protein FliG (**Fig. 6a**). This domain at the N-terminus of FlhF, which establishes the FlhF-FliG interaction, was termed the FliG interaction domain (FID).

We propose a model where FID-tethered FliG "catches" membrane-diffusing FliF proteins, which are likely being inserted into the membrane in an SRP-dependent co-translational manner *via* the canonical SecYEG pathway (reviewed in: (28, 29)). Whether the observation that FlhF constitutes the third member of SRP-GTPase family besides Ffh and FtsY is of functional relevance remains to be seen. So far, we have no reasonable evidence to believe that FlhF directly interacts with the SRP system, or serves in the co-translational insertion of any membrane protein. However, and given the uniform distribution of SecYEG machines along the cytoplasmic membrane (30), it is reasonable to assume that the insertion of FliF into the membrane can occur in close proximity to the pole (**Fig. 6a**). Hence, the suggested "diffusion-capture" mechanism, wherein FlhF anchors FliF via FliG and HubP to the cell pole, may primarily function to retain nascent flagellar building blocks at the cell pole and prevent their dispersion away from this crucial assembly site (**Figs. 6a,b**). This view is supported by our finding that removal of the FID instantaneously leads to delocalized flagella.

A surprising finding was that while the FlhF-FliG interaction allows engagement of FliG to FliF, it does not permit the interaction of FliG with its C-ring partners FliM/FliN (**Fig. 6b**). Thus, the interaction of FlhF and FliG provides an impediment for the latter to

6

1 complete C-ring assembly *via* FliM and FliN. This feature could provide a checkpoint:
2 FlhG, which stimulates the GTPase activity of FlhF (15, 16, 31, 32), interacts with
3 FliM/FliN *via* the N-terminus of the FliM protein (18, 19). Thus, we envision that
4 FliM/N complexes are only admitted to FlhF-bound FliF-FliG complexes when FlhG is
5 present (**Fig. 6c**). In such a way, FlhG can stimulate the GTPase activity of FlhF to
6 initiate a further round of FlhF-mediated "diffusion-capture" of the next flagellar
7 building blocks to the cell pole via the landmark protein HubP (**Figs. 6**).
8 In conclusion, our study elucidates the molecular framework governing how FlhF
9 coordinates the polar localization of the flagellum, working closely with the polar
10 landmark protein HubP and facilitating the assembly of flagellar MS-ring/C-ring
11 components at the cell pole.
12

Materials and Methods

14 **Protein production and purification.** Gene fragments encompassing the employed
15 proteins and their variants were amplified by polymerase chain reaction and inserted
16 into a pET24d vector (Novagen) *via* NcoI/XhoI restriction sites. The accession codes of
17 the genes encoding for the employed proteins are: *flhF*: Sputcn32_2561, *fliG*-polar:
18 Sputcn32_2575, *fliG*-lateral: Sputcn32_3475, *flhG*: Sputcn32_2560, *fliM*:
19 Sputcn32_2569, *fliN*: Sputcn32_2568, *fliF*: Sputcn32_2576 and *hubP*: Sputcn32_2442.
20 *Escherichia coli* strain BL21 (DE3) (Novagen) was employed for protein production,
21 with cells cultured in lysogeny broth medium (LB) supplemented with 1.5% (w/v) d(+)-
22 lactose monohydrate for 16 hours at 303 K. Cell pellets were resuspended at a ratio
23 of 10 ml of lysis buffer per gram of cells and then subjected to processing through an
24 M1-10L Microfluidizer (Microfluidics). The lysis buffer, comprising 20 mM Na-HEPES
25 at pH 8.0, 250 mM NaCl, 10 mM $MgCl_2$, and 10 mM KCl, was employed for this
26 purpose. The resulting lysate underwent clarification through centrifugation
27 (125,000g for 30 minutes at 277 K) using a Ti-45 rotor (Beckmann) and was
28 subsequently applied to a 1 ml HisTrap HP column (GE Healthcare). The column
29 underwent an initial wash with five column volumes of lysis buffer containing 40 mM
30 imidazole at pH 8.0. Protein elution was carried out in lysis buffer containing 500 mM
31 imidazole at pH 8.0. Following elution, the protein was concentrated to approximately
32 30 mg/ml using an Amicon Ultracel-10K (Millipore) and then subjected to size-
33 exclusion chromatography using either an S75/26–60 column or an S200/26–60 (GE
34 Healthcare) in the same buffer as before but without imidazole. Fractions containing
35 the protein were combined and concentrated as required.
36

37 **Pulldown assays.** StrepTagII pulldown assays conducted in order to study protein
38 interactions. Therefore, StrepII-tagged protein cultures and tested His-tagged protein
39 cultures (400 ml) were combined and lysed following the procedures outlined above.
40 Subsequently, the lysates were incubated with 30 μl of MagStrep Strep-Tactin XT
41 beads (iba Life Sciences) for 30 minutes at 4°C with gentle rotation. Following
42 centrifugation (4000 rpm, 5 minutes, 4°C), the supernatant was discarded, and the
43 beads underwent three washes with 500 μl of SEC Buffer, utilizing a magnetic rack.
44 The proteins bound to the beads were eluted using 200 μM D-Biotin in SEC buffer and
45 then subjected to analysis through SDS-PAGE.
46

GTPase activity assay. To assess the impact of interaction partners on the GTPase activity of FlhF, only proteins (including NG-FlhF) purified through size-exclusion chromatography were employed. Specifically, 1 nmol of NG-FlhF was incubated either alone or with 2 nmol of FlhG or HubP-C in a total reaction volume of 50 µL. The GTP concentration was 2 mM. The reaction proceeded for 60 minutes at 37°C without shaking. The reaction was stopped by the addition of 100 µl chloroform to each reaction, followed by boiling for 15 seconds at 98°C and rapid freezing in liquid nitrogen. Thereafter, each sample was thought and cleared by centrifugation (i.e., 13'000 RPM for 15 minutes in a benchtop centrifuge). Subsequently, the samples were analyzed by high-performance liquid chromatography (HPLC) on an Agilent 1260 Series system (Agilent Technologies) equipped with a Metrosep A Supp5 – 150/4.0 column (Metrohm International). The HPLC buffer, with a pH of 9.25 and comprising 90 mM $(NH_4)_2CO_3$, flowed at a rate of 0.6 ml/min. Nucleotides were detected at 260 nm.

Crystallization and structure determination. Crystallization was executed using the sitting-drop method at 20 °C with 250-nL drops containing an equal mixture of 1 mM protein and precipitation solutions. The specific crystallization conditions were 1.6 M sodium citrate, pH 6.5. Data collection took place under cryogenic conditions at the P13 beamline, Deutsches Eleketronen Synchrotron (DESY, Hamburg, Germany). Subsequently, the collected data were processed using XDS and scaled with XSCALE (33). Structural determination involved molecular replacement with PHASER (34), utilizing an Alphafold model (35). Manual building was carried out in COOT (36), and refinement was conducted using PHENIX 1.18.2 (37).

Yeast-Two Hybrid analysis. For Y2H interaction assays, plasmids expressing the FlhG bait protein, fused to the Gal4 DNA-binding domain, and prey proteins, fused to the Gal4 activation domain, were cotransformed into the reporter strain PJ69-4A (38). Y2H interactions were documented by spotting representative transformants in 10-fold serial dilution steps onto SC-Leu-Trp (-LT), SC-His-Leu-Trp (-HLT; HIS3 reporter), and SC-Ade-Leu-Trp (-ALT; ADE2 reporter) plates, which were incubated for 3 d at 30 °C. Growth on -HLT plates is indicative of a weak or moderate interaction, and only relatively strong interactions also permit growth on -ALT plates.

Western Blot Analysis. Western blot analysis was performed to check the stability and expression of the fusion proteins. The protein lysates of the respective strains were obtained from an exponentially growing culture and adjusted to the same optical density (OD600 of 10). For separation by SDS-PAGE, 10 µl of the samples were loaded onto the SDS-gel. The protein extracts were then transferred to membranes and visualized by Western blotting with antibodies against GFP as described previously (21). The respective antibodies are coupled to AP and CDP-Star chemiluminescent substrate (Roche, Switzerland) was used to generate a luminescent signal. The signal was detected using a Fusion-SL chemiluminescence imager (Peqlab, Erlangen, Germany).

Growth conditions and media. For all cloning experiments, *E. coli* cells were grown in LB medium or LB agar plates at 37°C containing antibiotics of the following

1   concentrations: 50 µg/ml kanamycin, 30 µg/ml chloramphenicol. Ectopic expression
2   was induced during exponential growth for 1 h from pBAD or pBBR-derived plasmids
3   with 0.05% L-arabinose and 0.5 mM IPTG. *S. putrefaciens* cells were grown in LB
4   medium or LB agar plates at 30°C. If necessary, media supplemented with 50 µg/ml
5   kanamycin, 300 µM 2,6-diaminopimelic acid, and/or 12% (w/v) sucrose were used for
6   conjugation.

7

8   **Strain Constructions.** The bacterial strains and plasmids used in this study are listed
9   in Supplementary Tables 2, 3 and 4, respectively. The primers used are indicated in
10 Supplementary Table 5. To introduce DNA into *S. putrefaciens*, *E. coli* WM3064 was
11 used. *E. coli* DH5αλ*pir* was used for cloning and experiments. For chromosomal
12 deletions in *S. putrefaciens* sequential crossover was conducted as previously
13 described (16) using derivatives of the plasmid pNPTS138-R6K (39). Corresponding
14 plasmids were constructed by Gibson assembly (40) by combining PCR-derived
15 fragments with EcoRV-digested pNPTS138-R6K.

16

17 **Hook Staining.** Fluorescent staining of hook structures (FlgE1-Cys) was essentially
18 carried out on exponentially growing cells as previously described (41). Briefly, the
19 strains were harvested from an exponentially growing culture and always handled
20 with cut pipette tips to avoid shear forces on the extracellular structures. After gentle
21 centrifugation at 3500 rpm for 5 minutes, the cell pellet was resuspended in 50 µl of
22 1x PBS. For staining, a maleimide ligate dye (Alexa Fluor 488-C5-maleimide fluorescent
23 dye; Thermo Fisher Scientific) was added and incubated in the dark for about 20
24 minutes. Afterwards cells were carefully washed twice with 1x PBS to remove
25 unbound ligate dye. The cells were the observed by fluorescence microscopy.

26

27 **Microscopy.** For imaging of samples, 2 µl of the respective strain were spotted on a
28 1% PBS-agarose (select agar, Invitrogen). Fluorescence microscopy was performed as
29 described previously (42), using a microscope set-up based on a Leica DMI 6000 B
30 inverse microscope (Leica), equipped with a pco.edge sCMOS camera (PCO), a
31 SPECTRA light engine (lumencor), an HCPL APO 63×/1.4–0.6 objective (Leica) using a
32 custom filter set (T495lpxr, ET525/50m; Chroma Technology) and the VisiView
33 software (Visitron Systems, Puchheim, Germany). Microscopy images were analyzed
34 by using ImageJ (v1.54g). Statistics and graph creation were done using Prism 9.5.1
35 (GraphPad software). Foci intensity analysis was made using BacStalk 1.8stable (22).

36

37 **Soft-agar spreading assays.** For *S. putrefaciens* soft-agar spreading assays, 2 µl of an
38 exponentially growing culture were spotted onto 0.25% LB agar plates (select agar,
39 Invitrogen). Plates were incubated for about 18 hours at 30°C. For documentation,
40 plates were scanned using an Epson V700 photo scanner. Different strains were
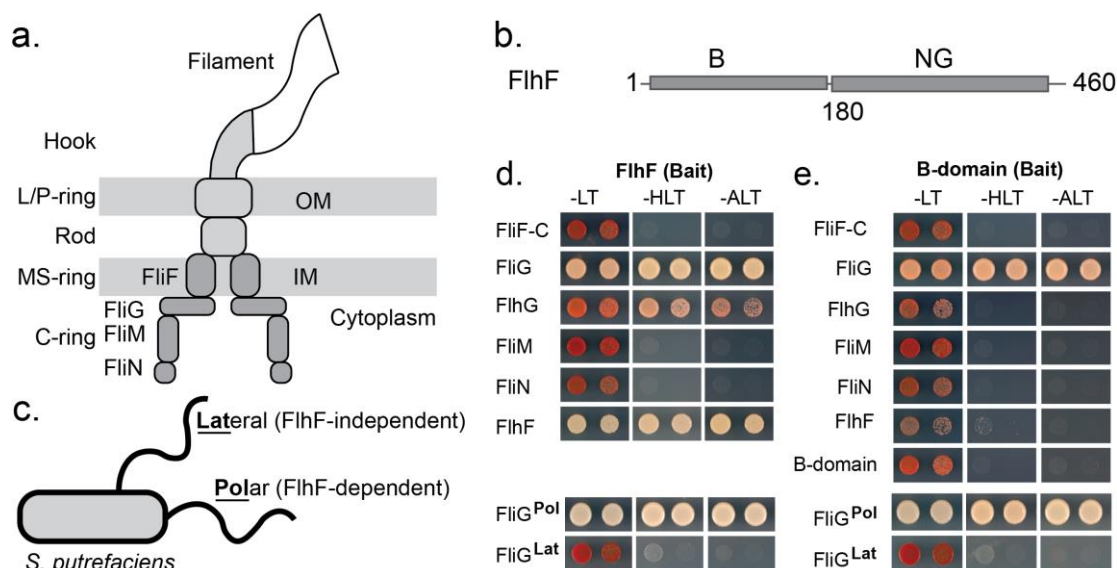41 always spotted on the same plate to ensure a direct comparison.

42

43

44 **Data availability.** Coordinates of the crystal structure have been deposited at the
45 Protein Data Bank with the accession code: 9EN1.

46

47 **The authors declare no conflicts of interest.**

9

Figures and figure legends.

Fig. 1. Essential role of FlhF's B-domain in interacting with FliG. a. Scheme of the architecture of the bacterial flagellum. **b.** Schematic representation of FlhF's domain structure. **c.** Scheme of the flagellation of the Gram-negative model organism *S. putrefaciens* featuring one polar and one lateral flagellum, whose localization is dependent and independent of FlhF, respectively. **d.** *Upper panel*: FlhF interacts with FliG while showing no interaction with FliF-C, FliM, and FliN from the polar system. *Lower panel*: FlhF exclusively associates with FliG from the polar flagellar system but not with FliG from the lateral system. **e.** *Upper panel*: The B-domain of FlhF is shown to interact with FliG, while no interaction is observed with FliF-C, FliM, and FliN of the polar system. *Lower panel*: The B-domain of FlhF demonstrates its ability to differentiate between the FliG proteins of the polar and lateral systems. The growth of cells, co-expressing the FlhF and FlhF-B bait proteinS and the indicated prey proteins, was assessed on SC-Leu-Trp (-LT), SC-His-Leu-Trp (-HLT; *HIS3* reporter) and SC-Ade-Leu-Trp (-ALT; *ADE2* reporter) plates.
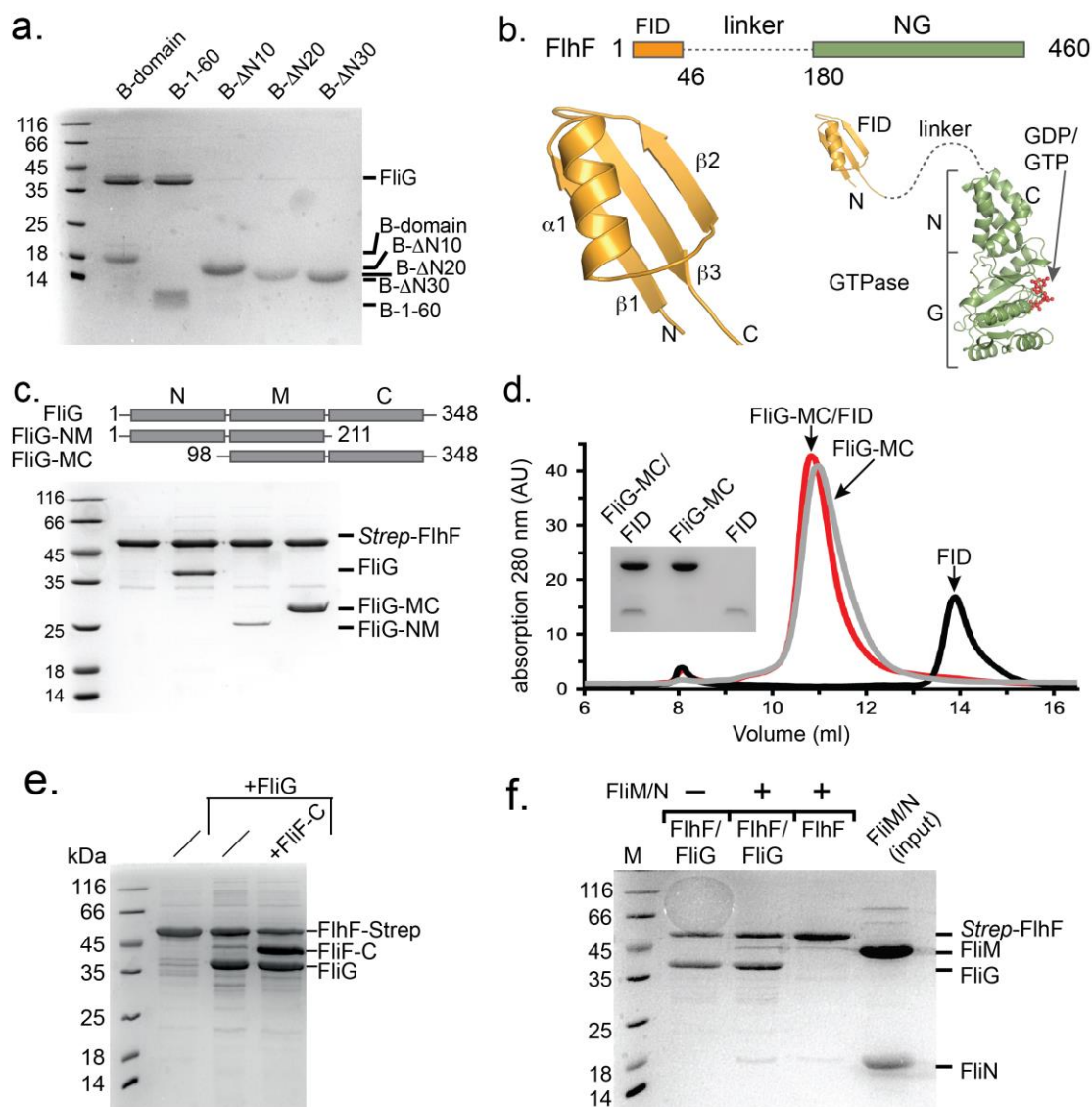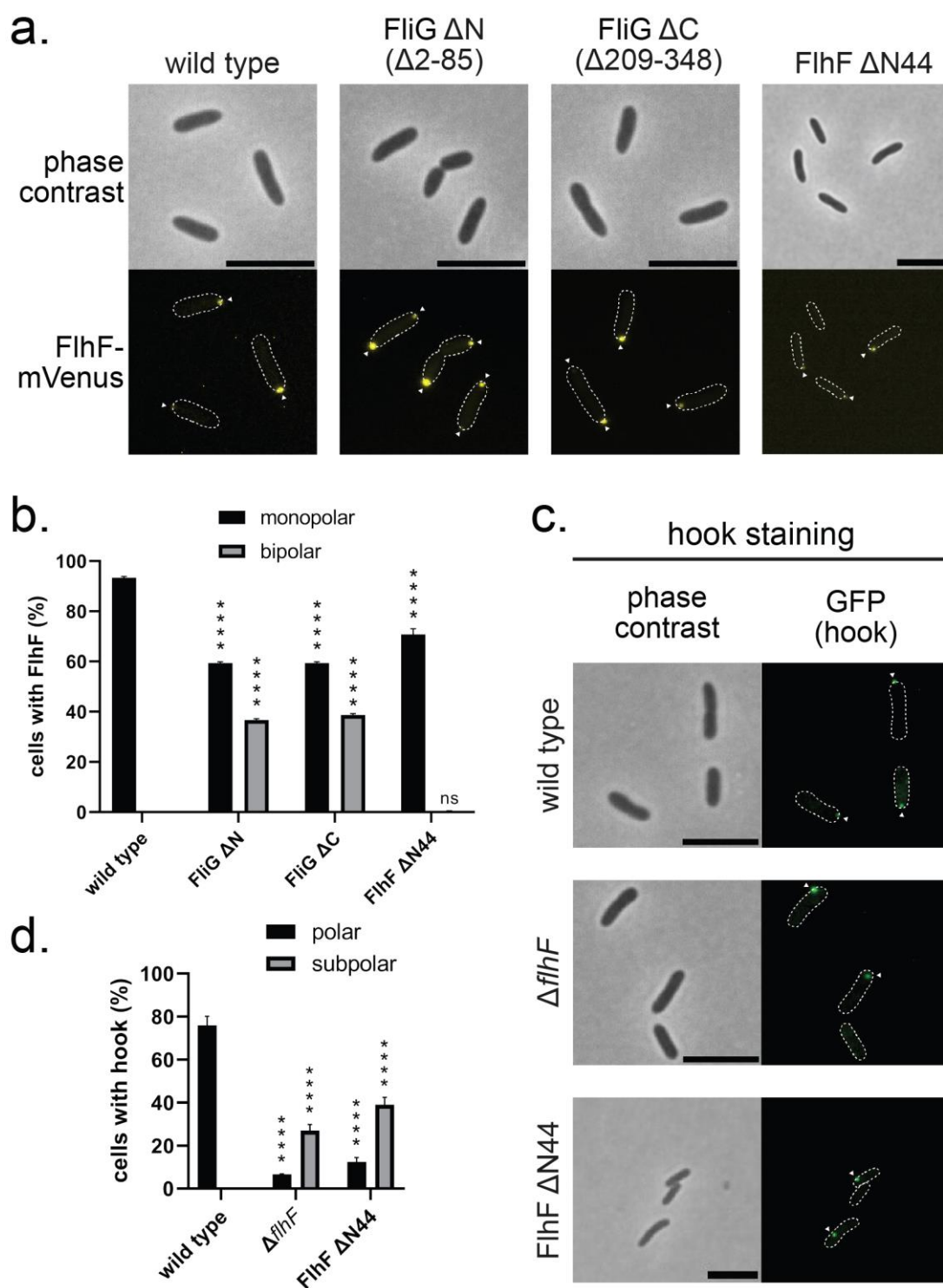
Fig. 2. Mechanistic dissection of the FlhF/FliG interaction. a. Coomassie-stained SDS-PAGE of an *in vitro* pulldown assay employing different StrepII-tagged variants of the B-domain as bait (the amino acid number are indicated) and full-length FliG as prey. **b.** Structural analysis of the FID-domain of FlhF. *Upper panel*: Revised scheme of the domain architecture of FlhF with the FliG-interacting domain (FID, orange), the structurally uncharacterized linker region (dashed line), followed by the NG domain (green). The domains are drawn to scale. *Lower panel, left*: X-ray structure of the FID domain of FlhF. *Lower panel, right*: X-ray structures of the FID domain (this study) and the GDP-bound state of the NG-domain (PDB-ID: 8R9R; (43)) from *S. putrefaciens* FlhF. The structurally uncharacterized linker is indicated by a dashed line, not drawn to scale. **c.** Coomassie-stained SDS-PAGE employing StrepII-tagged FlhF as bait and FliG and its variants (given in the panel above) as prey. **d.** Chromatogram of an analytical size exclusion chromatography of the FID domain of FlhF (black), the MC-domains of FliG (grey) and their complex (red). Coomassie-stained SDS-PAGE of the peak fraction of each run is shown in the inset. **e.** FlhF-tethered FliG can interact with FliF-C. Coomassie-stained SDS-PAGE employing StrepII-tagged FlhF as bait and FliG or FliG and FliF-C as prey. **f.** FlhF-tethered FliG cannot interact with FliM/N. Coomassie-

11

1 stained SDS-PAGE employing FliG-bound to StrepII-tagged FlhF as bait in the absence
2 and presence of FliM/N.
3
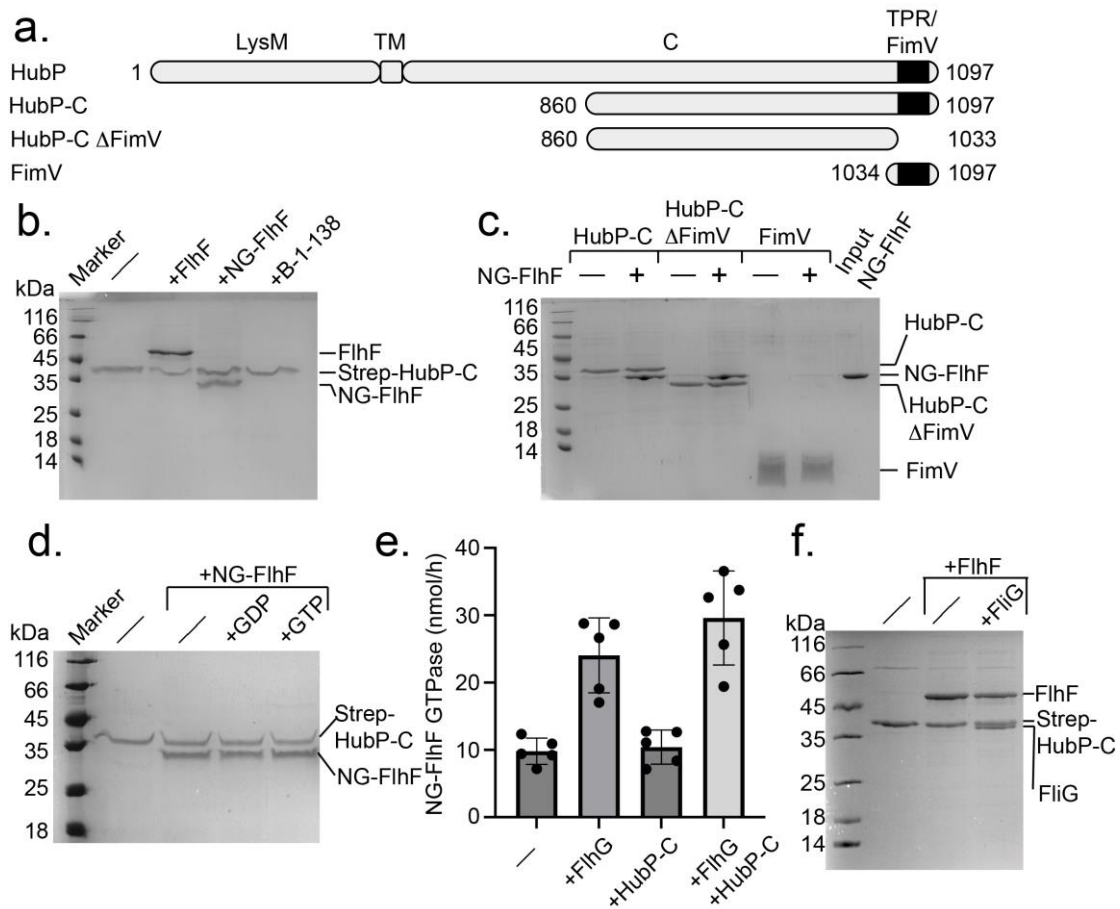
4
5 **Fig. 3. The NG-domain of FlhF interacts with the cytoplasmic region of HubP. a.**
6 Domain structure of the polar landmark protein HubP/FimV from S. putrefaciens and
7 constructs used in this study. **b.** Coomassie-stained SDS-PAGE employing StrepII-
8 tagged HubP-C as bait and FlhF, its NG-domain or the B-domain as prey. **c.** Coomassie-
9 stained SDS-PAGE employing StrepII-tagged HubP-C, StrepII-tagged HubP-C lacking
10 the C-terminal FimV domain or a StrepII-tagged FimV domain alone as bait and NG-
11 FlhF as prey. **d.** Coomassie-stained SDS-PAGE probing the impact of GDP or GTP on
12 interaction of StrepII-tagged HubP-C and NG-FlhF, acting as bait and prey,
13 respectively. **e.** GTPase activity of NG-FlhF in the presence of its stimulator FlhG, HubP-
14 C and the two together. The errors were calculated as standard deviation from 5
15 independent experiments, each shown as dot in the respective bars. **f.** Coomassie-
16 stained SDS-PAGE employing StrepII-tagged HubP-C as bait and FlhF alone and FlhF
17 and FliG.
18
19
20
21
22

Figure 4. The 44 aa N-terminal domain is required for FlhF function in *Shewanella*.
a) Microscopic images of the indicated *S. putrefaciens* strains expressing FlhF-mVenus. The top row shows the phase contrast images, while the bottom row shows the corresponding fluorescence images. Fluorescent FlhF-mVenus foci are marked with a white arrow. The scale bar equals 3 μm. **b)** Quantification of the FlhF-mVenus localization patterns in *S. putrefaciens* based on the microscopy images (biological triplicates, n ≥ 900) shown in a). Asterisks represent a p-value <0.0001 (Two-way ANOVA). **c.** Microscopic images of hook stains from the indicated *S. putrefaciens* strains with Alexa Fluor 488-C5-maleimide dye. The left row shows the phase contrast

13

1   images, while the right row shows the corresponding fluorescence images.
2   Fluorescent hooks are marked with a white arrow. The scale bar equals 3 µm. **d**
3   Quantification of the hook localization pattern in *S. putrefaciens* based on the
4   microscopy imagesshown in c) (biological triplicates, n ≥ 900). Asterisks represent a p-
5   value <0.0001 (Two-way ANOVA).
6
7
8
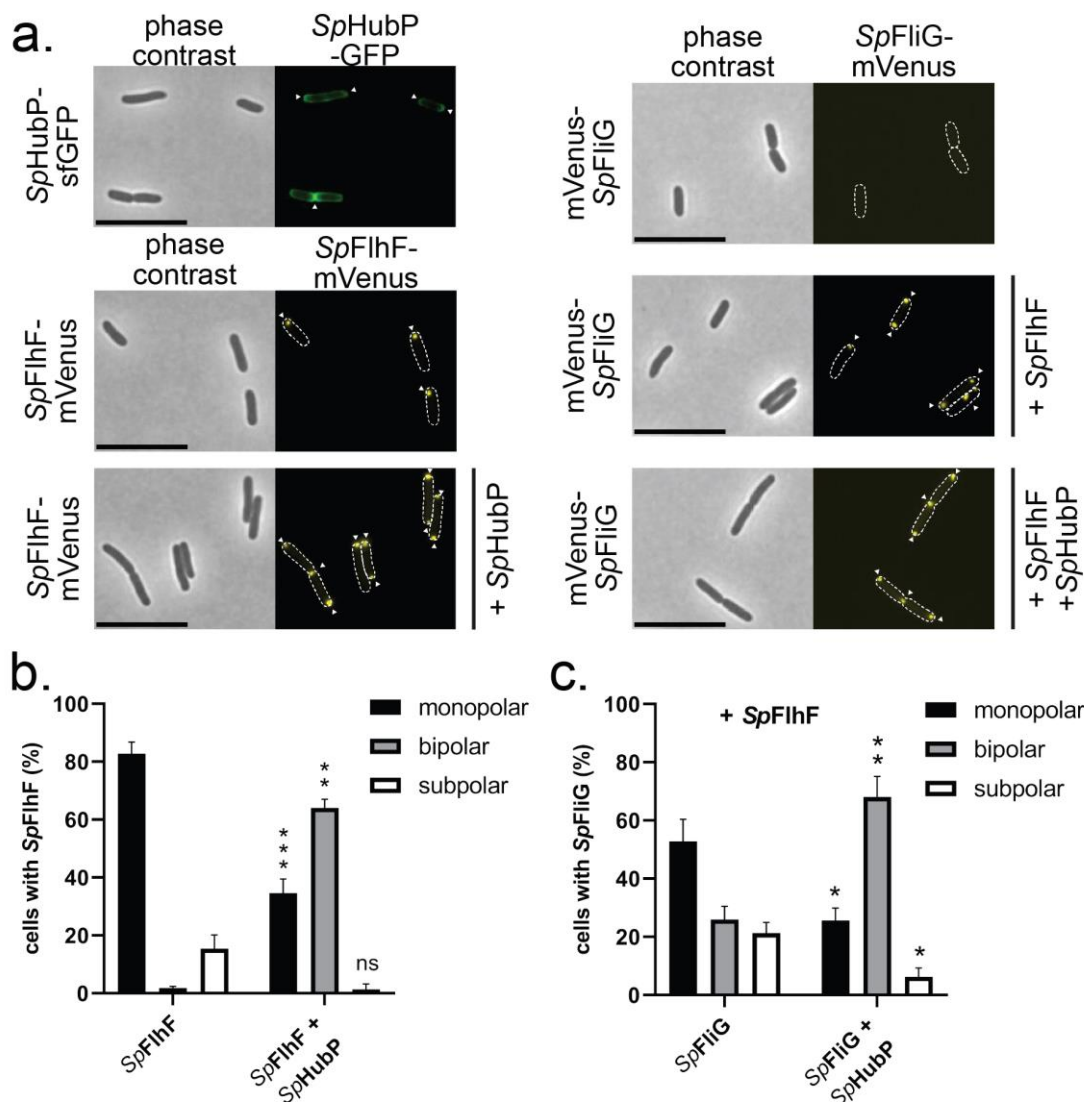
9
10   **Figure 5. The *Shewanella* HubP-FlhF-FliG recruitment cascade can be rebuilt in**
11   ***Escherichia coli.* a.** Microscopic images of the indicated *E. coli* DH5α strains containing
12   the expression plasmids for the wild-type version of HubP (*Sp*HubP) or fluorescently
13   tagged versions of *S. putrefaciens* HubP (*Sp*HubP), FlhF (*Sp*FlhF) or FliG (*Sp*FliG). The
14   left row shows the phase contrast images, while the right row shows the
15   corresponding fluorescence images. Fluorescent foci of the respective fluorescently
16   labeled protein are marked with a white arrow. The scale bar equals 5 µm. **b, c.**
17   Quantification of the localization pattern of *Sp*FlhF (**b**) or *Sp*FliG (**c**) in *E. coli* DH5α
18   based on the previous microscopy images (biological triplicates, n ≥ 900). Asterisks
19   represent a p-value of <0.001 (***) or <0.01 (**) or <0.05 (*) (Two-way ANOVA, ns =
20   not significant).

14
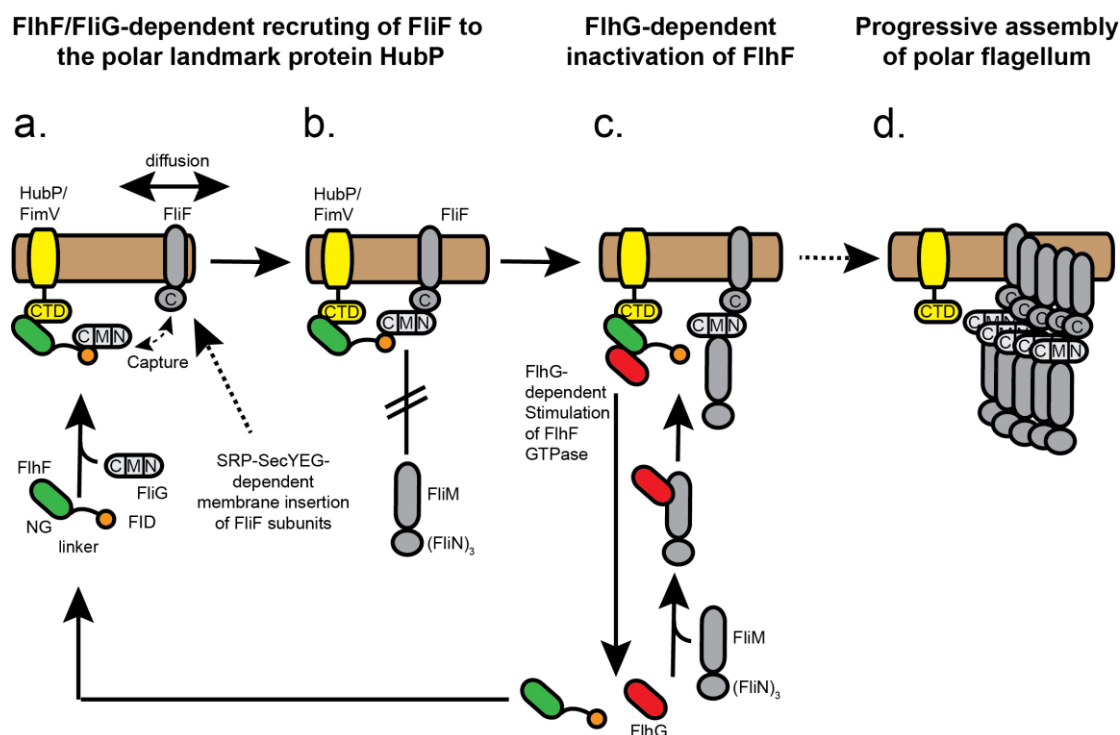
Figure 6. Model describing how FlhF establishes flagellar localization of polar flagella. The color code is: FlhF with its NG, linker and FID domains (green, black and orange, respectively), HubP/FimV (yellow), flagella building blocks (grey tones), FlhG (red) and the cytoplasmic membrane (light brown). Further descriptions are given in the discussion.

References

1. F. F. Chevance, K. T. Hughes, Coordinating assembly of a bacterial macromolecular machine. *Nat Rev Microbiol* **6**, 455-465 (2008).

2. S. Johnson *et al.*, Symmetry mismatch in the MS-ring of the bacterial flagellar rotor explains the structural coordination of secretion and rotation. *Nat Microbiol* **5**, 966-975 (2020).

3. S. Johnson *et al.*, Molecular structure of the intact bacterial flagellar basal body. *Nat Microbiol* **6**, 712-721 (2021).

4. P. K. Singh, G. Cecchini, T. Nakagawa, T. M. Iverson, CryoEM structure of a post-assembly MS-ring reveals plasticity in stoichiometry and conformation. *PLoS One* **18**, e0285343 (2023).

5. A. Kawamoto *et al.*, Native flagellar MS ring is formed by 34 subunits with 23-fold and 11-fold subsymmetries. *Nat Commun* **12**, 4223 (2021).

6. N. R. Francis, G. E. Sosinsky, D. Thomas, D. J. DeRosier, Isolation, characterization and structure of bacterial flagellar motors containing the switch complex. *J Mol Biol* **235**, 1261-1270 (1994).

7. S. Johnson *et al.*, Structural basis of directional switching by the bacterial flagellum. *Nat Microbiol* 10.1038/s41564-024-01630-z (2024).

8. J. S. Schuhmacher, K. M. Thormann, G. Bange, How bacteria maintain location and number of flagella? *FEMS Microbiol Rev* **39**, 812-822 (2015).

9. B. I. Kazmierczak, D. R. Hendrixson, Spatial and numerical regulation of flagellar biosynthesis in polarly flagellated bacteria. *Mol Microbiol* **88**, 655-663 (2013).

10. S. Kojima, H. Terashima, M. Homma, Regulation of the Single Polar Flagellar Biogenesis. *Biomolecules* **10** (2020).

11. J. C. Green *et al.*, Recruitment of the earliest component of the bacterial flagellum to the old cell division pole by a membrane-associated signal recognition particle family GTP-binding protein. *J Mol Biol* **391**, 679-690 (2009).

12. Y. Fukushima, M. Homma, S. Kojima, Interaction of FlhF, SRP-like GTPase with FliF, MS ring component assembling the initial structure of flagella in marine Vibrio. *J Biochem* **174**, 125-130 (2023).

13. G. Bange, G. Petzold, K. Wild, R. O. Parlitz, I. Sinning, The crystal structure of the third signal-recognition particle GTPase FlhF reveals a homodimer with bound GTP. *Proc Natl Acad Sci U S A* **104**, 13621-13625 (2007).

14. P. B. Carpenter, D. W. Hanlon, G. W. Ordal, flhF, a Bacillus subtilis flagellar gene that encodes a putative GTP-binding protein. *Mol Microbiol* **6**, 2705-2713 (1992).

15. G. Bange *et al.*, Structural basis for the molecular evolution of SRP-GTPase activation by protein. *Nat Struct Mol Biol* **18**, 1376-1380 (2011).

16. F. Rossmann *et al.*, The role of FlhF and HubP as polar landmark proteins in Shewanella putrefaciens CN-32. *Mol Microbiol* **98**, 727-742 (2015).

17. E. E. Arroyo-Pérez *et al.*, A conserved cell-pole determinant organizes proper polar flagellum formation. *bioRxiv* 10.1101/2023.09.20.558563 (2023).

18. J. S. Schuhmacher *et al.*, MinD-like ATPase FlhG effects location and number of bacterial flagella during C-ring assembly. *Proc Natl Acad Sci U S A* **112**, 3092-3097 (2015).

19. V. Blagotinsek *et al.*, An ATP-dependent partner switch links flagellar C-ring assembly with gene expression. *Proc Natl Acad Sci U S A* **117**, 20826-20835 (2020).

20. M. Schwan *et al.*, FlrA-independent production of flagellar proteins is required for proper flagellation in Shewanella putrefaciens. *Mol Microbiol* **118**, 670-682 (2022).

21. S. Bubendorfer *et al.*, Specificity of motor components in the dual flagellar system of Shewanella putrefaciens CN-32. *Mol Microbiol* **83**, 335-350 (2012).

22. S. Bubendorfer, M. Koltai, F. Rossmann, V. Sourjik, K. M. Thormann, Secondary bacterial flagellar system improves bacterial spreading by increasing the directional persistence of swimming. *Proc Natl Acad Sci U S A* **111**, 11485-11490 (2014).

23. N. Takekawa, S. Kwon, N. Nishioka, S. Kojima, M. Homma, HubP, a Polar Landmark Protein, Regulates Flagellar Number by Assisting in the Proper Polar Localization of FlhG in Vibrio alginolyticus. *J Bacteriol* **198**, 3091-3098 (2016).

24. E. E. Arroyo-Perez, S. Ringgaard, Interdependent Polar Localization of FlhF and FlhG and Their Importance for Flagellum Formation of Vibrio parahaemolyticus. *Front Microbiol* **12**, 655239 (2021).

25. R. N. Buensuceso *et al.*, The Conserved Tetratricopeptide Repeat-Containing C-Terminal Domain of Pseudomonas aeruginosa FimV Is Required for Its Cyclic AMP-Dependent and -Independent Functions. *J Bacteriol* **198**, 2263-2274 (2016).

26. S. Kojima *et al.*, Role of the N- and C-terminal regions of FliF, the MS ring component in Vibrio flagellar basal body. *J Bacteriol* **203** (2021).

27. H. Terashima *et al.*, Assembly mechanism of a supramolecular MS-ring complex to initiate bacterial flagellar biogenesis in Vibrio species. *J Bacteriol* **202** (2020).

28. P. Grudnik, G. Bange, I. Sinning, Protein targeting by the signal recognition particle. *Biol Chem* **390**, 775-782 (2009).

29. D. Akopian, K. Shen, X. Zhang, S. O. Shan, Signal recognition particle: an essential protein-targeting machine. *Annu Rev Biochem* **82**, 693-721 (2013).

30. B. Mayer *et al.*, Dynamics of Bacterial Signal Recognition Particle at a Single Molecule Level. *Front Microbiol* **12**, 663747 (2021).

31. C. J. Gulbronson *et al.*, FlhG employs diverse intrinsic domains and influences FlhF GTPase activity to numerically regulate polar flagellar biogenesis in Campylobacter jejuni. *Mol Microbiol* **99**, 291-306 (2016).

32. A. Kusumoto *et al.*, Collaboration of FlhF and FlhG to regulate polar-flagella number and localization in Vibrio alginolyticus. *Microbiology (Reading)* **154**, 1390-1399 (2008).

33. W. Kabsch, Xds. *Acta Crystallogr D Biol Crystallogr* **66**, 125-132 (2010).

34. A. J. McCoy *et al.*, Phaser crystallographic software. *J Appl Crystallogr* **40**, 658-674 (2007).

35. A. W. Senior *et al.*, Improved protein structure prediction using potentials from deep learning. *Nature* **577**, 706-710 (2020).

36. P. Emsley, K. Cowtan, Coot: model-building tools for molecular graphics. *Acta Crystallogr D Biol Crystallogr* **60**, 2126-2132 (2004).

37. D. Liebschner *et al.*, Macromolecular structure determination using X-rays, neutrons and electrons: recent developments in Phenix. *Acta Crystallogr D Struct Biol* **75**, 861-877 (2019).

38. P. James, J. Halladay, E. A. Craig, Genomic libraries and a host strain designed for highly efficient two-hybrid selection in yeast. *Genetics* **144**, 1425-1436 (1996).

39. J. Lassak, A. L. Henche, L. Binnenkade, K. M. Thormann, ArcS, the cognate sensor kinase in an atypical Arc system of Shewanella oneidensis MR-1. *Appl Environ Microbiol* **76**, 3263-3274 (2010).

40. D. G. Gibson, Synthesis of DNA fragments in yeast by one-step assembly of overlapping oligonucleotides. *Nucleic Acids Res* **37**, 6984-6990 (2009).

41. J. C. Hook *et al.*, A Proline-Rich Element in the Type III Secretion Protein FlhB Contributes to Flagellar Biogenesis in the Beta- and Gamma-Proteobacteria. *Front Microbiol* **11**, 564161 (2020).

42. M. J. Kuhn, F. K. Schmidt, B. Eckhardt, K. M. Thormann, Bacteria exploit a polymorphic instability of the flagellar filament to escape from traps. *Proc Natl Acad Sci U S A* **114**, 6340-6345 (2017).

43. A. Dornes, C. N. Mais, G. Bange, Structure of the GDP-bound state of the SRP GTPase FlhF. *Acta Crystallogr F Struct Biol Commun* **80**, 53-58 (2024).